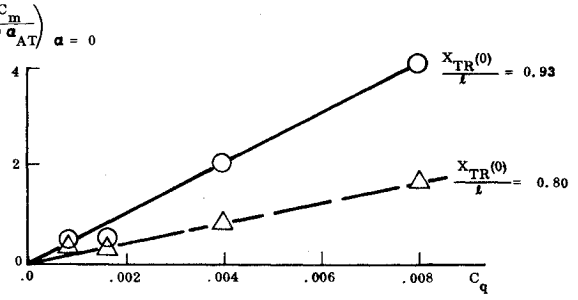

Fig. 5 Incremental blowing-induced stability derivative at $\alpha = 0$ as a function of blowing rate.

shown to exist in the α-range $\alpha_{AT} < \alpha < 4°$ for $\alpha_{AT} = 0°$, 1°, and 2° also would exist for other intermediate α_{AT}-values. It is hard to visualize any flow phenomenon that would invalidate this assumption. On the other hand, the local slopes used at $\alpha = \alpha_{AT}$ in obtaining the original fairing imply that $\partial C_m/\partial \alpha_{AT} = \partial C_m/\partial \alpha$; i.e., the transition movement derivative is assumed to be zero, $\partial x_{TR}/\partial \alpha = 0$, contrary to experimental evidence.[11]

Carpet-plotting the data[3] also for the other blowing rates gives the results shown in Fig. 4. At all blowing rates the destabilizing effect of asymmetric blowing is largest at small angles of attack near $\alpha_{AT} = 0$. One notices with some concern that the $C_m(\alpha)$-slope is negative for zero blowing rate, contrary to the measured effect of "free" asymmetric transition on a smooth solid model.[2] The reason for this anomaly is the "breathing" through the porous skin. It has been found that a porous skin model has substantially less $C_{N\alpha}$ than a solid model,[6,7] an effect that can be visualized to result from reduced streamline displacement due to in-flow through the high pressure side of the porous skin model. Here, in the case of the asymmetric porous skin configurations for $\alpha_{AT} = 1°$ and $\alpha_{AT} = 2°$, this would mean that the porous skin side is less effective in displacing the freestream and, as a consequence, a loss of leeside-to-windward-side pressure differential results. The associated gain in aft body normal force explains the statically stabilizing effect of asymmetric porous skin geometry shown in Fig. 4 for $C_q = 0$.

The incremental effects of blowing on the static stability derivative C_{m_α} at $\alpha = 0$, obtained from Fig. 4 for $X_{TR}(0)/ = 0.93$, are shown in Fig. 5. Also shown are the data for the other aft body asymmetric blowing configuration tested, i.e., $X_{TR}(0)/ = 0.80$. The results indicate that the destabilizing effect of asymmetric aft body blowing increases linearly with the blowing rate, and that the effect decreases in magnitude when the mean transition point, $X_{TR}(0)/l$, moves forward towards the center of gravity, $X_{CG}/l = 0.60$, all in agreement with the theoretical and experimental results shown in Ref. 2.

References

[1] Martellucci, A. and Neff, R. S., "The Influence of Asymmetric Transition on Re-Entry Vehicle Motion," *Journal of Spacecraft and Rockets*, Vol. 8, No. 5, May 1971, pp. 476–482.

[2] Ericsson, L. E., "Transition Effects on Slender Vehicle Stability and Trim Characteristics," *Journal of Spacecraft and Rockets*, Vol. 11, No. 1, Jan. 1974, pp. 3–10.

[3] Martellucci, A., "Asymmetric Transition Effects on the Static Stability and Motion History of a Slender Vehicle," SAMSO TR-70-141, 1970, Space and Missiles Systems Organization, Los Angeles Air Force Base, Calif.

[4] Reding, J. P. and Ericsson, L. E., "Dynamic Support Interference," *Journal of Spacecraft and Rockets*, Vol. 9, No. 7, July 1972, pp. 547–553.

[5] Eckstrom, D. J., "The Influence of Mass and Momentum Transfer on the Static Stability and Drag of a Slender Cone—An Experimental Correlation," LMSC/D051269, July 1968, Lockheed Missiles & Space Co., Sunnyvale, Calif.

[6] Wimberly, C. R., McGinnis, F. K., III, and Bertin, J. J., "Transpiration and Film Cooling Effects for a Slender Cone in Hypersonic Flow," *AIAA Journal*, Vol. 8, No. 6, June 1970, pp. 1032–1038.

[7] Ericsson, L. E. and Guenther, R. A., "Dynamic Instability Caused by Forebody Blowing," *AIAA Journal*, Vol. 11, No. 2, Feb. 1973, pp. 231–233.

[8] Bertin, J. J., McCloskey, M. H., Stalmach, C. J., and Wright, R. L., "Effect of Mass-Addition Distribution and Injectant on Heat Transfer and Transition Criteria," AIAA Paper 72-183, San Diego, Calif., 1972.

[9] Jecmen, D. M., Reding, J. P., and Ericsson, L. E., "An Application of Automatic Carpet Plotting to Wind-Tunnel Data Reduction," *Journal of Spacecraft and Rockets*, Vol. 4, No. 3, March 1967, pp. 408–410.

[10] Jecmen, D. M., "Automatic Carpet Plotting," LMSC 80563, Jan. 1967, Lockheed Missiles & Space Co., Sunnyvale, Calif.

[11] Ericsson, L. E., "Correlation of Attitude Effects on Slender Vehicle Transition," *AIAA Journal*, Vol. 12, No. 4, April 1974.

Cylindrical Wing-Body Configurations for Space-Limited Applications

D. E. SWANSON* AND C. T. CROWE†
Washington State University, Pullman, Wash.

Nomenclature

a_{-1} = residue
b = wing span
C_L = coefficient of lift
L = lift force
r = body radius
S = cross-sectional area
U_∞ = freestream velocity
V_n = normal component of velocity
w = complex potential
x, y = abscissa and ordinate in crossflow plane, respectively
Y = side force
z = streamwise coordinate
Z = complex variable in crossflow plane
Z_w = location of the wing in the Z_3-plane
α = angle of attack
γ = vortex strength distribution
ζ = distance along vortex sheet
Λ = aspect ratio
ξ = complex function for the body axis
ρ = freestream density

Subscripts

1, 2, 3 = first, second, and third complex planes
B = base plane of vehicle
∞ = freestream

Introduction

THE design of a vehicle with cruise capability which can be stored in a limited space usually involves the use of lifting surfaces which can be hinged or folded to satisfy the volume constraint. Several concepts for hinged and foldable wings are well-known. One such concept is the "scissor wing" which is hinged about its leading edge and swings out from a cavity in the fuselage. The primary disadvantage of this design is the reduction in load-carrying capacity and over-all utility of the vehicle due to the cavity in the fuselage. Another concept is the parawing, which is a flexible wing suspended by lines from

Received June 25, 1973; revision received September 10, 1973.
Index category: LV/M Aerodynamics.

* Graduate Student, Master's degree, Department of Mechanical Engineering.
† Associate Professor, Department of Mechanical Engineering. Member AIAA.

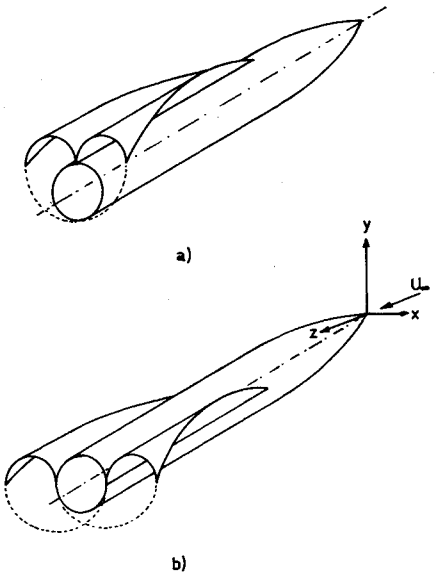

Fig. 1 Cylindrical wing-body configurations.

the fuselage. The parawing is difficult to deploy at high speeds and has a characteristically poor lift-drag ratio precluding high performance cruise operation. A third design possibility features flat wings hinged near the fuselage which, in the folded position, rest against the surface of the fuselage. The disadvantage of this particular design is the limited span available, especially if the vehicle is to be stored in a cylinder. The hinged wing, however, can be used effectively as a control surface. Another design[1] which has been proposed in connection with re-entry vehicles consists of conical-shaped wings mounted on a half-cone fuselage. By mounting these wings on hinges at the fuselage, they can be folded against the fuselage to facilitate vehicle storage.

A promising design concept for hinged wings, studied by Crowell and Crowe,[2] is illustrated in Fig. 1a. The wings consist of two tapered semicylinders which hinge along the top of the fuselage. When not deployed, the two wings wrap around the side of the cylindrical fuselage. Theory predicts this wing-body configuration has a lift-curve slope 35% higher than that of a flat wing of the same span mounted on the top of the fuselage. Also, deployment is relatively simple and reliable. The major disadvantage is that the span is limited to twice the fuselage diameter and the lift developed may not satisfy design requirements.

The span and the attendant lift can be increased considerably by mounting the semicylindrical wings on the side of the fuselage as illustrated in Fig. 1b. In this case the span is three times the body diameter which, according to slender body theory, would result in a lift more than twice that obtained from the top-hinged wings at the same angle of attack. When not deployed the wings would wrap, one upon the other, around the underside of the fuselage. The purpose of this Note is to determine analytically the lift characteristics of such a wing-body configuration.

Analytic Approach

Slender body theory is used to predict the lift force. A slender body is characterized by small changes in cross-sectional area in the streamwise direction, such as a pointed slender fuselage or a low aspect-ratio wing. Expanding the velocity potential in powers of a slenderness parameter (such as body thickness or aspect ratio) and retaining the lowest order terms, Ward[3] shows that: 1) The flow at infinity for any general slender body becomes axisymmetric and equal to the flow at infinity around an equivalent axisymmetric body of revolution; and 2) Near the slender body, the flow differs from that around the equivalent body of revolution by a two-dimensional constant density crossflow part that makes the tangency condition satisfied. Thus, the flowfield at any section along the body can be subdivided into a velocity component parallel to the body axis and a crossflow component which can be treated as a two-dimensional ideal flow.

Ward[3] shows that the lift and side force on a slender body is obtained from

$$Y+iL=-i\rho U_\infty{}^2\int_{C_B} w(Z)\,dZ+\rho U_\infty{}^2[\xi'(z_B)S(z_B)+\xi(z_B)S'(z_B)] \quad (1)$$

where $w(Z)$ is the complex potential of the crossflow The contour integral is evaluated at the station corresponding to the wing's maximum span (base plane). The variable $\xi(z)$ is a complex function for the center of the body's cross-sectional area, $S(z)$, with respect to the z-axis. $S'(z_B)$ is the rate of change of the body's cross-sectional area at the base plane which is zero for the wing-body configuration under study here. Evaluating the contour integral by the residue theorem, the equation for lift can be written as

$$L=\rho U_\infty{}^2\,Im[2\pi a_{-1}(z_B)-i\alpha S(z_B)] \quad (2)$$

where a_{-1} is the residue of the complex potential for the crossflow.

The tangency condition requires that the normal velocity component at the surface be equal to $\xi'(z_B)$, the velocity at infinity being zero. It is more straightforward, however, to let the normal velocity component be zero and the velocity at infinity be $-\xi'(z_B)$. The residue is the same for both cases.

The cross section of the wing-body configuration at the base plane is shown in Fig. 2a. It is assumed that the side-slip angle is zero so the flowfield at infinity is a rectilinear flow of magnitude α in the positive y-direction, the complex potential being $w=-i\alpha Z_1$. The flowfield can be constructed by representing the wings as vortex sheets. Then for each vortex on a wing, there must be a corresponding vortex of the opposite strength reflected inside the body to guarantee that the cylindrical fuselage is a streamline.

The analysis can be simplified by transforming the fuselage into a vertical slit using the transformation

$$Z_2=Z_1-(r^2/Z_1) \quad (3)$$

where r is the radius of the fuselage. The wings transform into near circular arcs connected to the body at the origin as shown in Fig. 2b. The complex potential at infinity remains unchanged. The flowfield can be solved in this plane by again representing the wings as symmetric vortex sheets, the fuselage automatically being a streamline by maintaining flow symmetry about the y-axis.

It was found, however, that the computation was facilitated by inverting the Z_2-plane onto a third plane

$$Z_3=1/Z_2 \quad (4)$$

The resulting configuration is shown in Fig. 2c. The fuselage is transformed into two slits along the y_3-axis, both extending to infinity. The wings becomes two slits which originate at $\pm 3/8r$ on

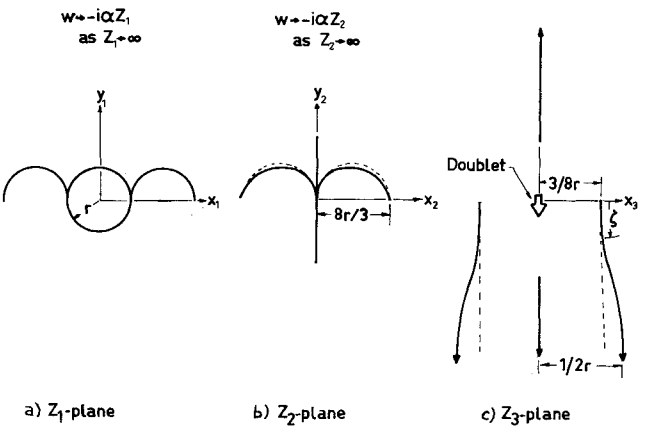

Fig. 2 Transformations of the crossflow plane.

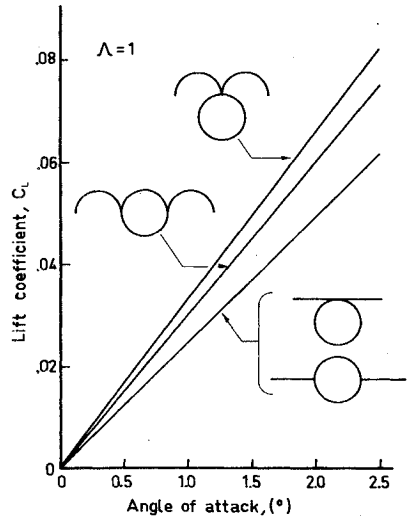

Fig. 3 Comparison of lift coefficient for cylindrical and flat wing-body combinations.

the x_3-axis and asymptotically approach $\pm 1/2r$ as y_3 decreases toward infinity. The intersection point between the wing and fuselage in the Z_2-plane is thereby greatly expanded in the Z_3-plane and leads to a more detailed representation of the complex potential in this region. The rectilinear flow at infinity in the Z_2-plane becomes a doublet pointing downward at the origin in the Z_3-plane.

The two wings in the Z_3-plane can be represented by two symmetric vortex sheets. Since the y_3-axis must be a streamline, the vortex strength at corresponding y_3's on both wings must have the same magnitude but opposite sense, according to the reflection principle. The complex potential resulting from the two vortex sheets and the doublet at the origin can be expressed as

$$w(Z_3) = i\int_0^\infty \gamma(\zeta)\ln\left[\frac{Z_3 - Z_w(\zeta)}{Z_3 + \bar{Z}_w(\zeta)}\right]d\zeta - \frac{i\alpha}{Z_3} \tag{5}$$

where ζ is the distance along the wing (vortex sheet) starting at $\pm 3/8r$, $\gamma(\zeta)$ is the vortex strength distribution and $Z_w(\zeta)$ is the complex variable describing the location of the wing in the Z_3-plane. The velocity component normal to wings must be zero in order that the wings be streamlines so the following condition

$$V_n = Im[Z_w'(\zeta)(dw/dZ_3)|_{Z_w}] = 0 \tag{6}$$

must be satisfied everywhere along the wing. This leads to an integral equation for $\gamma(\zeta)$ which was solved numerically by subdividing the vortex sheet into a series of discrete vortices. Having determined the vortex strength distribution, the residue is obtained by expanding the complex potential in a Laurent series about $Z_3 = 0$ and writing Z_3 as a function of Z_1. The result is

$$a_{-1}(z_B) = i\alpha r^2 - 2i\int_0^\infty \gamma(\zeta)(Re[Z_w]/|Z_w|^2)\,d\zeta \tag{7}$$

which gives a numerical value for the residue of

$$a_{-1}(Z_B) = 5.40\,i\alpha r^2 \tag{8}$$

The wings in the Z_2-plane do not deviate significantly from the semicircles represented by dashed lines in Fig. 2. If, indeed, the wings were semicircles, the inversion mapping would have yielded the two semi-infinite slits indicated also by the dashed lines in the Z_3-plane. It would then have been possible to transform the wings onto the x-axis using the Schwartz-Christoffel transformation, the fuselage still being two slits along the y-axis. In this case the doublet at the origin in the Z_3-plane would have become a doublet on the y-axis directed in the negative y-direction so the flowfield analysis would have reduced to the simple problem of a doublet near a wall. Since the actual wings in the Z_2-plane approximate semicircles, the flowfield solution for the semicircular wings was obtained and the residue evaluated to serve as a check on the above result. The residues differed by less than 5%, that for the actual wing being the smaller of the two.

The lift force is predicted by substituting the residue into Eq. 2. The result is

$$L = 9.80\pi\rho U_\infty{}^2 r^2\alpha \tag{9}$$

The wing span is six times the body radius so the lift force can be written as

$$L = (9.80\pi/36)\rho U_\infty{}^2 b^2\alpha \tag{10}$$

The lift coefficient, then, is

$$C_L = 1.71\Lambda\alpha \tag{11}$$

and the lift curve slope has the value of

$$C_{L_\alpha} = 1.71\Lambda \tag{12}$$

Spreiter[4] has shown that flat wings of the same span mounted on the side of the fuselage have a lift curve slope of 1.41Λ. Thus, the cylindrical wings produce over 20% more lift than the flat wings at the same angle of attack.

It is interesting to compare graphically the predicted lift coefficient vs angle of attack for cylindrical and flat wing-body combinations as illustrated in Fig. 3. Both the top-mounted and side-mounted cylindrical wings outperform their flat-wing counterparts. The highest lift curve slope is obtained for the top-mounted cylindrical wings. However, the highest lift is obtained for the side-mounted wings since the span is increased from two to three times the body diameter. The comparatively higher lift curve slope of the cylindrical wings suggests their suitability for high performance cruise vehicles which can be packaged in a limited space. Experimental verification of the predicted lift characteristics and measurements of other aerodynamic parameters, such as drag, are necessary before the relative merits of cylindrical wings can be realistically assessed.

References

[1] Fournier, P. G., "Aerodynamic Characteristics at Low Speed of a Reentry Configuration Having Rigid, Tractable, Conical Lifting Surfaces," TN D-622, 1960, NASA.

[2] Crowell, K. R. and Crowe, C. T., "Prediction of the Lift and Moment on a Slender Cylinder-Segment Wing-Body Combination," *Journal of the Royal Aeronautical Society*, Vol. 77, No. 750, 1973, pp. 295–298.

[3] Ward, G. N., *Linearized Theory of High Speed Flow*, Cambridge Univ. Press, Cambridge, Mass., 1955.

[4] Spreiter, J. R., "The Aerodynamic Forces on Slender Plane and Cruciform-Wing and Body Combination," Rept. 962, 1950, NACA.

Simulation of Real-Gas Effects for Mars Entry

JAMES L. HUNT,* ROBERT A. JONES,* AND RAYMOND E. MIDDEN†
NASA Langley Research Center, Hampton, Va.

Nomenclature

A = reference area, $\pi R_B{}^2$
C_D = drag coefficient, $D/q_\infty A$

Received July 19, 1973; revision received September 6, 1973.
Index categories: Supersonic and Hypersonic Flow; Entry Vehicles and Landers; Entry Vehicle Testing.

* Aerospace Technologist, Hypersonic Aircraft Systems Research Branch, Hypersonic Vehicles Division.
† Aerospace Technologist, Gas Radiation Section, Space Systems Division.